PAPER

Check for updates

Photocatalytic activity of silicon-based nanoflakes for the decomposition of nitrogen monoxide†

Hiroshi Itahara, [ID] *[a] Xiaoyong Wu,[b] Haruo Imagawa, [ID] [a] Shu Yin,[b] Kazunobu Kojima,[b] Shigefusa F. Chichibu[b] and Tsugio Sato[b]

The photocatalytic decomposition of nitrogen monoxide (NO) was achieved for the first time using Si-based nanomaterials. Nanocomposite powders composed of Si nanoflakes and metallic particles (Ni and Ni_3Si) were synthesized using a simple one-pot reaction of layered $CaSi_2$ and $NiCl_2$. The synthesized nanocomposites have a wide optical absorption band from the visible to the ultraviolet. Under the assumption of a direct transition, the photoabsorption behavior is well described and an absorption edge of *ca.* 1.8 eV is indicated. Conventional Si and SiO powders with indirect absorption edges of 1.1 and 1.4 eV, respectively, exhibit considerably low photocatalytic activities for NO decomposition. In contrast, the synthesized nanocomposites exhibited photocatalytic activities under irradiation with light at wavelengths >290 nm (<4.28 eV). The photocatalytic activities of the nanocomposites were confirmed to be constant and did not degrade with the light irradiation time.

Introduction

The discovery of strong visible luminescence emitted from porous silicon (Si)[1] has stimulated research into the synthesis of Si nanomaterials for optoelectronic applications. Si nanomaterials are also expected to be applicable as photocatalytic materials for hydrogen generation by water-splitting[2–7] and as anode materials for Li-ion batteries.[8,9] Useful nanomaterials are typically in the form of porous or hollow particles and nanotubes that have free nanospaces and large surface-to-volume ratios. Various synthetic routes for photocatalytic Si nanomaterials have been investigated, such as chemical etching of Si,[5] magnesioreduction of natural clay,[6] molten-salt-induced exfoliation of natural clay[7] and a self-templating method by the co-precipitation of Si and a salt.[3] On the other hand, conventional layered siloxene $(Si_6O_3H_6)$[10] is known as a Si-based bulk material with a direct band gap,[11] although photocatalytic applications have not been reported, with the exception of a recent study on exfoliated siloxene nanosheets.[12]

We have developed a simple and scalable synthetic method that provides nanomaterial containing agglomerates of Si-based nanoflakes with slit-like nanopores.[13–15] The method uses a solid-state exfoliation reaction of layered $CaSi_2$ and transition metal chlorides as raw materials. We have verified that the formation of the nanoflakes is based on the extraction of Ca from the layered $CaSi_2$ by the formation of $CaCl_2$ as a driving force,[13] where $CaSi_2$[16,17] has a layered structure with alternate stacking of a planar Ca layer and a monolayer Si sheet composed of six-membered Si rings. The reaction of $CaSi_2$ and $TaCl_5$ provides Ca-bridged siloxene nanoflakes with thicknesses of *ca.* 15 nm (hereafter referred to as Ca-siloxene) and a typical molar ratio of Ca : Si = 0.1 : 2. Ca-Siloxene has a structure composed of Ca atoms bridging adjacent Kautsky-type siloxene[10] monolayer sheets (six-membered Si rings connected *via* O–Si–O). Ca-Siloxene exhibits composition-directed tunable light absorptivity[15] and stable performance as an anode for Li-ion batteries.[18] On the other hand, the reaction of $CaSi_2$ and $NiCl_2$ provides a nanocomposite powder composed of similar Si nanoflakes, Ni and nickel silicide (*i.e.*, Ni_3Si, Ni_2Si or NiSi) particles. Excellent performance as an anode for Li-ion batteries was observed for these nanocomposites,[13,14] where Ni and nickel silicide were considered to function as the conductive medium.

In this study, we focused on the application of nanocomposites derived from $CaSi_2$ as a catalyst material for the photocatalytic decomposition of nitrogen monoxide (NO), which is a typical air pollutant. In contrast to TiO_2, which is a representative photocatalyst for the decomposition of pollutants,[19,20] the study of Si or siloxene for NO decomposition has not been reported to date. Here we report on the photoabsorption and photocatalytic properties of these nanocomposites composed of Si nanoflakes and metallic particles.

[a] Toyota Central R&D Labs., Inc., 41-1 Yokomichi Nagakute, Aichi 480-1192, Japan. E-mail: h-itahara@mosk.tytlabs.co.jp
[b] Institute of Multidisciplinary Research for Advanced Materials, Tohoku University, 2-1-1 Katahira, Aoba-ku, Sendai 980-8577, Japan
†Electronic supplementary information (ESI) available: Measurement procedures of photocatalytic activities using a continuous reactor. See DOI: 10.1039/c7dt01682d

Experimental

The nanocomposites containing Si nanoflakes were prepared by a previously described method.[13,14] Reagents of $CaSi_2$ (99.5%, <32 μm, Rare Metallic Co.) and anhydrous $NiCl_2$ (99.9%, Kojundo Chemical Lab.) were used as starting materials. A mixture of *ca.* 200 mg of $CaSi_2$ and $NiCl_2$ (molar ratio of 1 : 1) powder was loaded into a BN crucible under an Ar atmosphere in a glove box. The crucible was placed inside a stainless-steel cell (inner volume of *ca.* 10 cm^3) and then heated at 300, 400 or 500 °C for 5 h, followed by cooling to room temperature to produce samples denoted as S-300, 400 and 500, respectively. The reaction products were washed with dimethylformamide (Wako Pure Chemical Industries, Ltd) to remove the $CaCl_2$ by-product. Finally, the obtained powders were dried in a vacuum at 80 °C for 5 h. As a reference sample, Ca-siloxene was prepared by the method described in a previous report.[15] The synthesis procedure was essentially the same as that for the nanocomposites except that a different chloride source ($TaCl_5$: 99.99%, Kojundo Chemical Laboratory) and washing solvent (anhydrous ethanol: Wako Pure Chemical Industries, Ltd) were used, and the synthesis temperature was set at 215 °C. The nominal molar ratio of $CaSi_2$: $TaCl_5$ was 1 : 1.

The crystalline phases of the synthesized samples were identified using powder X-ray diffraction (XRD; Rigaku RINT-TTR). Microstructures were analyzed using scanning electron microscopy (SEM; Hitachi High-Technologies SU3500) and scanning transmission electron microscopy (STEM; JEOL, JEM-2010FEF). Elemental mapping images of the synthesized samples were obtained using SEM with energy-dispersive X-ray (EDX; Horiba EX-370) spectroscopy. N_2 adsorption isotherms (Quantachrome Instruments Nova 3000) were measured to determine the specific surface areas of the samples from Brunauer–Emmett–Teller (BET) plots.

Diffuse reflectance spectroscopy (Jasco V-670) measurements were performed over a 2 mm diameter of each sample. The reflectivity data were processed under the Kubelka–Munk formalism[21] and absorption edges were estimated from Tauc plots.[22] The photocatalytic activity for NO decomposition was determined using a continuous reactor as described in our previous report[23] (Fig. S1†). Here, the evaluation was followed by the established procedures in the Japanese Industrial Standard.[24] The photocatalytic activity of the samples was characterized by the decrease in the concentration of NO gas at the outlet of the reactor. The powder samples were packed in the groove of the holder (20 × 20 × 0.2 mm^3). A constant flow (200 mL min^{-1}) of 1 ppm NO–50 vol% air (balance N_2) was used as a test gas. Prior to light irradiation, the test gas was flown continuously for 10 min to achieve a balance between diffusion and adsorption. The wavelength of the irradiated light was set to >290 nm (450 W high-pressure mercury lamp equipped with Pyrex glass as a filter) or >400 nm with the ultraviolet emission filtered out.

As a standard photocatalytic material, we evaluated a commercial TiO_2 powder (P25, Degussa; ST-01, Ishihara Industry Co. Ltd) composed of 70% anatase and 30% rutile. Commercial Si (1–2 μm, >97%, Strem Chemicals, Inc.) and SiO powders (<38 μm, 99.9%, Kojundo Chemical Lab.) were also evaluated as Si-based reference samples.

Results and discussion

Fig. 1 shows XRD patterns for the raw $CaSi_2$ powder, synthesized powder samples, and reference commercial powders. The peaks attributed to $CaSi_2$ were absent in the XRD patterns for synthesized Ca-siloxene[15] (Fig. 1(b)), and S-300, 400 and 500 samples (Fig. 1(c)–(e)). The XRD peaks in the pattern for the S-300 sample were assigned to Si and Ni, while those for S-400 and 500 samples were assigned to Si, Ni and Ni_3Si. Amorphous Si nanoflakes were also present in all the samples, as described below (Fig. 2). This is consistent with the
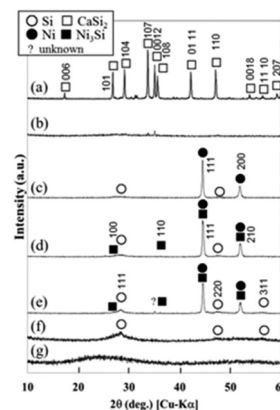
Fig. 1 Powder XRD patterns for (a) $CaSi_2$ (raw material), (b) Ca-siloxene, synthesized (c) S-300, (d) 400 and (e) 500 samples, and (f) commercial Si and (g) SiO.
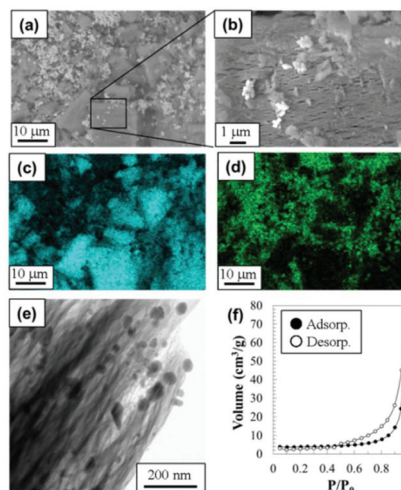
Fig. 2 (a, b) SEM images, SEM-EDX elemental mapping image for (c) Si and (d) Ni, (e) STEM image and (f) N_2 adsorption isotherm for the synthesized S-400 sample.

previously reported results,[13] in which the Si nanoflakes were formed by extracting Ca from layered $CaSi_2$ and simultaneously exfoliating the layered structure. At elevated synthesis temperatures, a larger amount of Si crystallized with the diamond c-Si structure and also formed Ni_3Si by reaction with Ni, but excess Si still remained as amorphous Si nanoflakes. The amount of Ni and Ni_3Si would be ~50 mol% because $NiCl_2$ was not observed for the reaction products before washing. Commercial Si powder was identified as c-Si with low crystallinity (Fig. 1(f)). No crystalline phases could be assigned for the commercial SiO powder (Fig. 1(g)); however, SiO was reported to be a mixture of nanosized elemental Si and amorphous SiO_2.[25]

Fig. 2 shows the microstructure and N_2 adsorption isotherm for the S-400 sample. Particles with sizes less than 1 μm were distributed on and around grains with sizes on the order of micrometers (Fig. 2(a) and (b)). EDX elemental mapping images (Fig. 2(c) and (d)) indicated that the particles were Ni-rich, and Si was dominant in the grains. In addition, the grains were agglomerates of the Si nanoflakes, as reported in previous papers.[13,14] Considering the XRD pattern shown in Fig. 1(d), the particles were assigned to Ni and Ni_3Si. The average molar ratio of Ca : Si was 0.07 : 2 for the Si nanoflakes, which is close to that of Ca-siloxene (0.1 : 2). The streak-like contrasts in the STEM image (Fig. 2(e)) were Si nanoflakes with thicknesses of ca. 10 nm, as reported previously,[13,14] while the round shaped dark contrasts in the image were Ni and Ni_3Si particles.

Ni and Ni_3Si particles with diameters of 5–50 nm were present in contact with the Si nanoflakes. The N_2 adsorption isotherm (Fig. 2(f)) of the sample showed an IUPAC H3 type hysteresis loop,[26] which is typically observed for materials with slit-like pores. The gaps between the assembled Si nanoflakes acted as slit-like nanopores for the adsorption of N_2. The microstructures of the S-300 and 500 samples were similar to that of the S-400 sample.

Fig. 3(a) shows diffuse reflectance spectra of the S-300–500 samples, Ca-siloxene, and the commercial Si and SiO powders. Fig. 3(b) and (c) show Tauc plots[22] of Kubelka–Munk absorption (K/S)[21] as a function of photon energy $(h\nu)$ processed with the reflectance data under the assumptions of direct and indirect transitions, respectively. The synthesized samples (Ca-siloxene, S-300, 400 and 500 samples) exhibited a broad absorption tail ranging from visible to ultraviolet wavelengths. The absorption edge was ca. 1.8 eV under the assumption of a direct transition, as shown in Fig. 3(b). The commercial Si and SiO powders appeared to have identical absorption edges (Fig. 3(b)). However, assuming an indirect transition (Fig. 3(c)) resulted in absorption edges of ca. 1.1 and 1.4 eV for the Si and SiO powders, respectively, while reasonable Tauc plots were not obtained for the synthesized samples. These absorption edges are close to those of c-Si (1.1 eV) and amorphous Si (ca. 1.8 eV (ref. 27 and 28)). The determined absorption edge is consistent with that reported for SiO, which was considered to be a mixture of nanosized elemental Si and amorphous SiO_2.[25] The Tauc plot in Fig. 3(b) had a flexion point at around 4 eV for the S-400 and 500 samples, which suggests that the
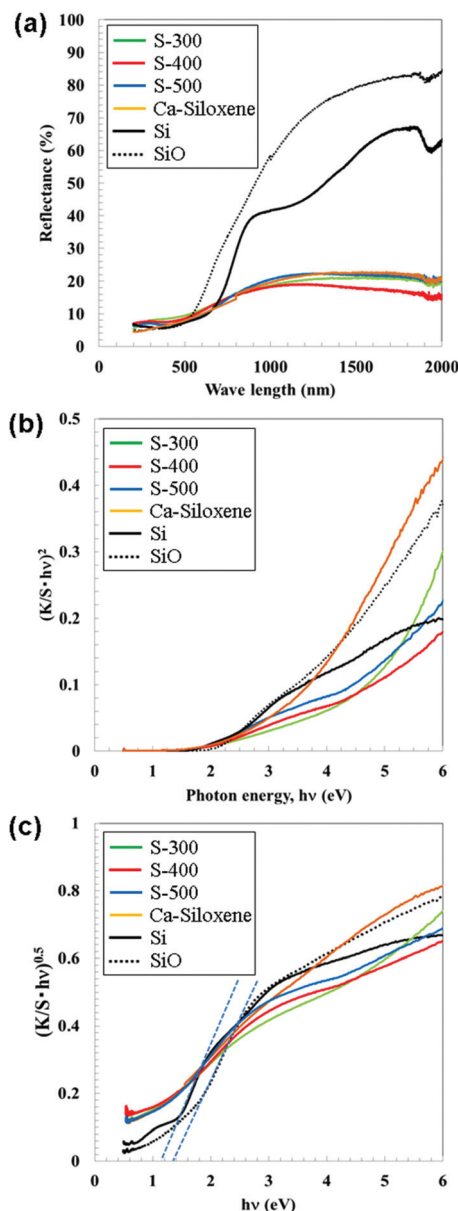

Fig. 3 (a) Diffuse reflectance spectra, and (b, c) Tauc plots of Kubelka–Munk absorption (K/S) as a function of photon energy $(h\nu)$ under the assumption of (b) direct and (c) indirect transition for reference samples (Si, SiO, Ca-siloxene) and synthesized samples (S-300, 400 and 500).

samples have at least two constituents that absorb the light. Metallic compounds of Ni and Ni_3Si[29,30] would not contribute to the absorption. Accordingly, the absorption around 2–3 eV is assigned to low crystallinity c-Si present in the synthesized samples because both the amount of light absorption (Fig. 3(b)) and the XRD peak intensities of Si (Fig. 1(d) and (e)) were increased with the synthesis temperatures. The absorption of light with photon energies higher than 4 eV would be attributable to the Si nanoflakes. For the S-300 sample with weak XRD peaks for Si, the Tauc plot in Fig. 3(b) was similar to that for Ca-siloxene and light absorption due to c-Si was not clearly observed.
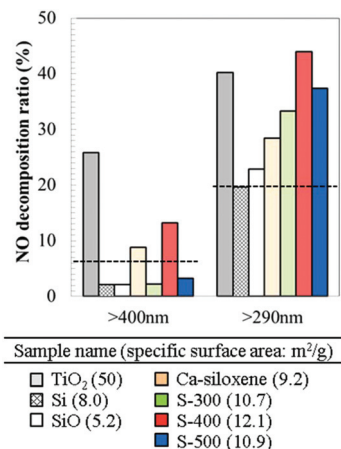
Fig. 4 Nitrogen monoxide decomposition ratio over reference samples (TiO$_2$, Si, SiO, Ca-siloxene) and synthesized samples (S-300, 400 and 500). The dotted lines indicate the blank data (ratio observed without a catalyst).

Fig. 4 shows the photocatalytic NO decomposition ratio for the synthesized and reference samples. Approximately 20% of NO was decomposed by the ultraviolet rays, even without a photocatalyst;[23] therefore, the commercial Si and SiO powders exhibited considerably low photocatalytic properties. On the other hand, Ca-siloxene and the S-300–500 samples showed considerably high NO decomposition ratios. The formation of singlet oxygen ($^1O_2$) was observed as one of the active species for the single phase Ca-siloxene powders,[31] as is the case with photocatalysis over TiO$_2$.[32] Thus, it is expected that the degradation products would be N$_2$ and HNO$_3$ as clarified for the TiO$_2$ catalyst.[33,34]

S-300–500 samples showed a higher NO decomposition ratio than the single phase Ca-siloxene powders. Metallic particles on photocatalyst materials are generally considered to facilitate the separation of photoinduced charges.[35,36] The electrical resistivity of Ca-siloxene and the S-300–500 samples measured using powder compacts were 1.9×10^7, 1.0×10^3, 1.0×10^3 and 1.1×10^3 Ω cm, respectively. Ni[37] and bulk Ni$_3$Si[29] show electrical resistivity at room temperature of 6.9×10^{-6} and 9.4×10^{-5} Ω cm, respectively, suggesting that most Si nanoflakes in the S-300–500 samples would come into contact with Ni and Ni$_3$Si particles. The exact positions of conduction and valence bands of the Si nanoflakes are hard to be determined by both theoretical and experimental methods because Si nanoflakes are powders with low crystallinity: *e.g.*, the photoemission yield spectroscopy measured in air gives only a rough estimation of the ionization potentials. However, the measured ionization potential and the absorption edge (Fig. 3) suggested that the valence band of the Si nanoflakes located around 3 eV below the vacuum level while the Fermi level of Ni locates further below (~4 eV). Thus, the photoinduced charges in the Si nanoflakes could easily migrate to Ni. A systematic study by changing the ratio of Si nanoflakes and metallic particles would be necessary to prove the exact effect of co-existing metallic phases as a future study.

Under irradiation with light at wavelengths >400 nm (<3.1 eV; light without ultraviolet), the S-400 sample and Ca-siloxene both exhibited weak but observable photocatalytic activity. The photocatalytic activity was reproducibly observed and was independent of the synthetic batch. All of the S-300–500 samples had absorption edges of *ca.* 1.8 eV (*ca.* 690 nm, Fig. 3(b)), which indicates that these samples have similar potential to function as photocatalysts with light irradiation of >400 nm wavelength. The difference in the observed photocatalytic activities among the S-300–500 samples may originate from the different degrees of charge separation associated with the different mixing ratios of Si nanoflakes to metallic particles and their particle sizes. These differences were evident from the observed phases (Fig. 1) and the specific surface areas (see the inset table in Fig. 4). Furthermore, photocatalytic NO decomposition under the light containing ultraviolet rays (>290 nm) for the S-400 sample did not degrade over time, as shown in Fig. 5. This is clearly different from the results reported for photocatalytic water-splitting over siloxene nanosheets, whereby the activity was rapidly degraded.[12] It is also noted that a part of test gas passed without coming into contact with the catalyst materials in the current reactor (Fig. S1†) and thus the NO decomposition ratio of 40% was the highest. In addition, because it is a continuous reaction system, the decomposition ratio strongly related to the flow rate and the concentration of NO gas. The characterization system in the present research was similar to that of the Japanese Industrial Standard.[24] At a high flow rate (about 200 ml min^{-1}) of NO gas in this study, the decomposition ratio of 40% would be considerably high. On the other hand, the rapid response of photocatalytic reactions is indicated in Fig. 5.

A previous report[38] on TiO$_2$ photocatalysts prepared under various synthetic conditions showed that the specific surface area of the samples was an important factor for enhancement of the photocatalytic activity for NO decomposition. The S-300–500 samples prepared in the present work exhibited comparable or higher photocatalytic NO decomposition ratios when compared to commercial TiO$_2$ (Fig. 4), even though their
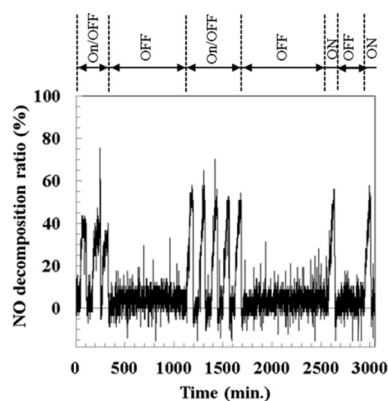

Fig. 5 Nitrogen monoxide decomposition ratio as a function of light (>290 nm) irradiation time for the synthesized sample S-400.

specific surface areas were approximately 5 times smaller than that of TiO_2 (see the inset table in Fig. 4). Thus, the nanocomposites synthesized in this study have significant potential for application as photocatalysts. A solid-state exfoliation reaction using layered $CaSi_2$ has the potential to produce, in principle, nanocomposites composed of Si nanoflakes and various types of electroconductive particles. In addition, such a top-down one-pot process using micrometer-sized raw materials has advantages in terms of being a simple and scalable synthetic route.

Conclusions

The photoabsorption properties and photocatalytic activity for NO decomposition were examined for nanocomposites containing Si nanoflakes and metallic particles derived from layered $CaSi_2$ as a raw material. The Si nanoflakes were *ca.* 10 nm thick and the metallic particles formed were Ni and Ni_3Si. The nanocomposite had a broad absorption tail ranging from visible to ultraviolet wavelengths, due mainly to the Si nanoflake content. The synthesized nanocomposites exhibited high photocatalytic NO decomposition ratios that were far superior to those of conventional Si and SiO powders. Under light irradiation (>290 nm), the nanocomposites exhibited comparable or higher activity than a commercial TiO_2 powder used as a standard photocatalytic material. The photocatalytic activity of the synthesized nanocomposite for NO decomposition was not degraded with time. It is considered that the presence of metallic particles in the nanocomposite may facilitate photoinduced charge separation. Here, we have demonstrated that one-pot synthesis of nanocomposites can exhibit enhanced photocatalytic activity for NO decomposition, thereby suggesting a practical strategy for the production of high performance Si-based photocatalyst materials.

Acknowledgements

Notes and references

1 L. T. Canham, *Appl. Phys. Lett.*, 1990, **57**, 1046.
2 H. Bahruji, M. Bowker and P. R. Davies, *Int. J. Hydrogen Energy*, 2009, **34**, 8504–8510.
3 F. Dai, J. Zai, R. Yi, M. L. Gordin, H. Sohn, S. Chen and D. Wang, *Nat. Commun.*, 2014, **5**, 3605.
4 F.-B. Zhang, S.-F. Lv, J.-X. Jiang and Y. Ni, *Appl. Organomet. Chem.*, 2014, **28**, 826–830.
5 T. Li, J. Li, Q. Zhang, E. Blazeby, C. Shang, H. Xu, X. Zhang and Y. Chao, *RSC Adv.*, 2016, **6**, 71092–71099.
6 Y. J. Jang, J. Ryu, D. Hong, S. Park and J. S. Lee, *Chem. Commun.*, 2016, **52**, 10221–10224.
7 J. Ryu, Y. J. Jang, S. Choi, H. J. Kang, H. Park, J. S. Lee and S. Park, *NPG Asia Mater.*, 2016, **8**, e248.
8 U. Kasavajjula, C. Wang and A. J. Appleby, *J. Power Sources*, 2007, **163**, 1003–1039.
9 X. Su, Q. Wu, J. Li, X. Xiao, A. Lott, W. Lu, B. W. Sheldon and J. Wu, *Adv. Energy Mater.*, 2014, **4**, 1300882.
10 A. Weiss, G. Beil and H. Meyer, *Z. Naturforsch., B: Anorg. Chem. Org. Chem.*, 1979, **34**, 25.
11 L. Brus, *J. Phys. Chem. B*, 1994, **98**, 3575–3581.
12 S. Li, H. Wang, D. Dandan Li, X. Zhang, Y. Wang, J. Xie, J. Wang, Y. Tian, W. Ni and Y. Yi Xie, *J. Mater. Chem. A*, 2016, **4**, 15841–15844.
13 S. Y. Oh, H. Imagawa and H. Itahara, *Chem. – Asian J.*, 2014, **9**, 3130–3135.
14 S.-Y. Oh, H. Imagawa and H. Itahara, *J. Mater. Chem. A*, 2014, **2**, 12501.
15 H. Imagawa, N. Takahashi, T. Nonaka, Y. Kato, K. Nishikawa and H. Itahara, *J. Mater. Chem. A*, 2015, **3**, 9411–9414.
16 H. Schäfter, B. Eisenmann and W. Mü ller, *Angew. Chem., Int. Ed. Engl.*, 1973, **12**, 694.
17 E. Zintl, *Angew. Chem.*, 1939, **52**, 1.
18 H. Imagawa and H. Itahara, *Dalton Trans.*, 2017, **46**, 3655–3650.
19 K. Hashimoto, H. Irie and A. Fujishima, *Jpn. J. Appl. Phys.*, 2005, **44**, 8269–8285.
20 S. Yin, *J. Ceram. Soc. Jpn.*, 2015, **123**, 823–834.
21 P. Kubelka and F. Munk, *Z. Tech. Phys.*, 1931, **12**, 593.
22 J. Tauc, R. Grigorovici and A. Vancu, *Phys. Status Solidi*, 1966, **15**, 627.
23 S. Yin, H. Hasegawa, D. Maeda, M. Ishitsuka and T. Sato, *J. Photochem. Photobiol., A*, 2004, **163**, 1–8.
24 Japanese Standards Association, Japanese Industrial Standard R1701-1, 2004.
25 K. Schulmeister and W. Mader, *J. Non-Cryst. Solids*, 2003, **320**, 143–150.
26 J. Rouquerol, F. Rouquerol and K. Sing, *Adsorption by Powders and Porous Solids: Principles, Methodology and Applications*, 1998.
27 K. Tanaka, K. Nakagawa, A. Matsuda, M. Matsumura, H. Yamamoto, S. Yamasaki, H. Okushi and S. Iizima, *Jpn. J. Appl. Phys.*, 1980, **20**, 267–273.
28 F. Ishihara, H. Uji, T. Kamimura, S. Matsumoto, H. Higuchi and S. Chichibu, *Jpn. J. Appl. Phys.*, 1995, **34**, 2229–2234.
29 M. Amiotti, A. Borghesi, G. Guizzetti and F. Nava, *Phys. Rev. B: Condens. Matter*, 1990, **42**, 8939–8946.
30 A. Gheorghiuy, S. Senemaudy, E. Belin-Ferrey, Z. Dankhaziyz, L. Magaud-Martinagex and D. A. Papaconstantopoulosk, *J. Phys.: Condens. Matter*, 1996, **8**, 719–728.
31 H. Imagawa, *et al.*, to be submitted.
32 S. Yin, B. Liu, P. Zhang, T. Morikawa, K. Yamanaka and T. Sato, *J. Phys. Chem. C*, 2008, **112**, 12425–12431.
33 J. S. Dalton, P. A. Janes, N. G. Jones, J. A. Nicholson, K. R. Halam and G. C. Allen, *Environ. Pollut.*, 2002, **120**, 415–422.

34 M. Anpo, *In Recent DeVelopments on Visible Light Response Type Photocatalysts*, NTS, Tokyo, 2002, p. 9.

35 M. Anpo and M. Takeuchi, *J. Catal.*, 2003, **216**, 505–516.

36 S. Yin and T. Sato, *J. Photochem. Photobiol., A*, 2005, **169**, 89–94.

37 C. J. Smithells, *Metals Referece Book*, Butter Worths, 5th edn, 1967.

38 S. Yin, Y. Aita, M. Komatsu, J. Wang, Q. Tang and T. Sato, *J. Mater. Chem.*, 2005, **15**, 674–682.